THE JOURNAL OF BIOLOGICAL CHEMISTRY VOL. 287, NO. 12, pp. 8944–8953, March 16, 2012
Published in the U.S.A.

Sometimes It Takes Two to Tango

CONTRIBUTIONS OF DIMERIZATION TO FUNCTIONS OF HUMAN α-DEFENSIN HNP1 PEPTIDE[*S]

Received for publication, December 9, 2011, and in revised form, January 19, 2012 Published, JBC Papers in Press, January 23, 2012, DOI 10.1074/jbc.M111.332205

Marzena Pazgier[‡§1], Gang Wei[‡¶1,2], Bryan Ericksen[‡1], Grace Jung[‖], Zhibin Wu[‡], Erik de Leeuw[‡], Weirong Yuan[‡], Henryk Szmacinski[**], Wei-Yue Lu[¶], Jacek Lubkowski[§3], Robert I. Lehrer[‖], and Wuyuan Lu[‡4]**

*From the [‡]Institute of Human Virology and **Department of Biochemistry and Molecular Biology, University of Maryland School of Medicine, Baltimore, Maryland 21201, the [§]Macromolecular Assembly Structure and Cell Signaling Section, NCI, National Institutes of Health, Frederick, Maryland 21702, the [¶]School of Pharmacy, Fudan University, Shanghai 201203, China, and the [‖]Department of Medicine, David Geffen School of Medicine, UCLA, Los Angeles, California 90095*

Background: Human α-defensin 1 (HNP1) is a small but functionally versatile antimicrobial peptide that exists as dimers and oligomers.
Results: Destabilization of HNP1 dimer significantly impairs its ability to kill *S. aureus*, inhibit anthrax lethal factor, and bind HIV-1 gp120.
Conclusion: Dimerization and oligomerization are important for many activities of HNP1.
Significance: The molecular basis of functional versatility of human α-defensins is better understood.

Human myeloid α-defensins called HNPs play multiple roles in innate host defense. The Trp-26 residue of HNP1 was previously shown to contribute importantly to its ability to kill *S. aureus*, inhibit anthrax lethal factor (LF), bind gp120 of HIV-1, dimerize, and undergo further self-association. To gain additional insights into the functional significance of dimerization, we compared wild type HNP1 to dimerization-impaired, *N*-methylated HNP1 monomers and to disulfide-tethered obligate HNP1 dimers. The structural effects of these modifications were confirmed by x-ray crystallographic analyses. Like the previously studied W26A mutation, *N*-methylation of Ile-20 dramatically reduced the ability of HNP1 to kill *Staphylococcus aureus,* inhibit LF, and bind gp120. Importantly, this modification had minimal effect on the ability of HNP1 to kill *Escherichia coli*. The W26A and MeIle-20 mutations impaired defensin activity synergistically. N-terminal covalent tethering rescued the ability of W26A-HNP1 to inhibit LF but failed to restore its defective killing of *S. aureus*. Surface plasmon resonance studies revealed that Trp-26 mediated the association of monomers and canonical dimers of HNP1 to immobilized HNP1, LF, and gp120, and also indicated a possible mode of tetramerization of HNP1 mediated by Ile-20 and Leu-25. This study demonstrates that dimerization contributes to some but not all of the many and varied activities of HNP1.

Defensins are 2–5-kDa disulfide-stabilized antimicrobial peptides that are involved in various aspects of innate immunity and host defense (1–6). They include three subfamilies known as α-, β-, and θ-defensins. Human α-defensins 1–3, also known as human neutrophil peptides or HNP1–3, make up 5–7% of total neutrophil protein (7, 8), and α-defensin HNP4 is present in much smaller amounts (9, 10). Two enteric α-defensins (HD5 and HD6) found in small intestinal Paneth cells complete the roster of human α-defensins (11, 12). α-Defensins are active against bacteria, fungi, and viruses. Their antimicrobial properties against Gram-negative bacteria, such as *Escherichia coli*, are generally attributed to the disruption of microbial membranes (13, 14). Their antiviral mechanisms are more varied (15). α-Defensins HNP1–3 and HD5 also neutralize bacterial toxins, including anthrax lethal factor (LF)[5] (16–18), and exhibit lectin-like properties toward glycosylated proteins (18, 19). In addition, α-defensins are capable of binding host cell receptors, playing an important role in innate inflammatory and adaptive immune responses (20). The structural features that impart this functional versatility of α-defensins are only partially known (6).

α-Defensins have a triple-stranded β-sheet structure with three intra-molecular disulfides. They dimerize and may form higher order oligomers (21, 22). As shown in the crystal structure of HNP1 (Fig. 1), two monomers associate via the central (2nd) β-strands (anti-parallel) to form a symmetric dimer (18). The dimer interface is stabilized by four backbone-backbone H-bonds donated reciprocally by the NH groups of Ile-20 and Thr-18 to the carbonyl C=O groups of Thr-18 and Ile-20. In

* This work was supported, in whole or in part, by National Institutes of Health Grants AI072732 and AI061482 (to W. L.) and by the Intramural Research Program, NCI, Center for Cancer Research (to J. L.).

[S] This article contains supplemental Table S1, Figs. S1 and S2, additional text, and additional references.

The atomic coordinates and structure factors (codes 3HJD and 3HJ2) have been deposited in the Protein Data Bank, Research Collaboratory for Structural Bioinformatics, Rutgers University, New Brunswick, NJ (http://www.rcsb.org/).

[1] These authors contributed equally to this work.

[2] Supported by National Natural Science Foundation of China Grant 30701060.

[3] To whom correspondance may be addressed. E-mail: lubkowsj@mail.nih.gov.

[4] To whom correspondence may be addressed: Tel.: 410-706-4980; Fax: 410-706-7583; E-mail: wlu@ihv.umaryland.edu.

[5] The abbreviations used are: LF, lethal factor; Tricine, *N*-[2-hydroxy-1,1-bis(hydroxymethyl)ethyl]glycine; RU, response unit; Acm, acetamidomethyl; Abu, α-aminobutyric acid.

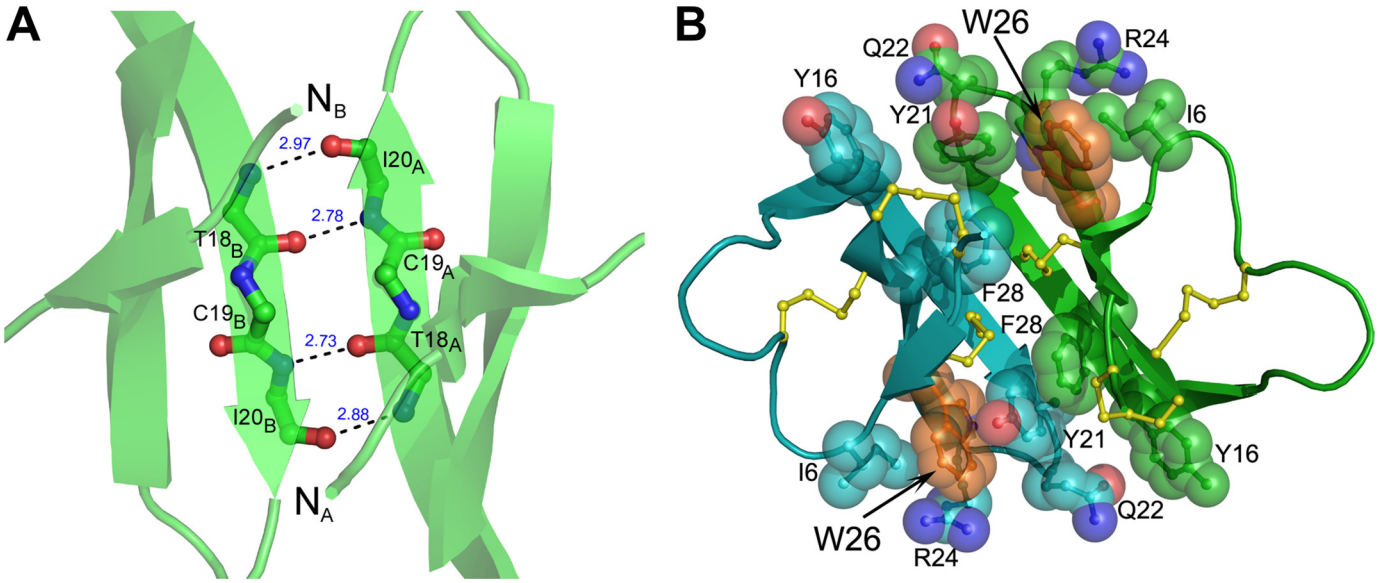

FIGURE 1. **Dimer interface of HNP1.** *Left panel,* inter-molecular H-bonding network at the dimer interface of HNP1. Thr-18 and Ile-20 of monomer A (*right panel*) each donate one backbone H-bond to (⟨NH→O = C⟩) and accept one backbone H-bond from (⟨C=O←HN⟩) Ile-20 and Thr-18, respectively, of monomer B (*left panel*). *N*-Methylation of Ile-20 breaks the two short H-bonds (2.73 and 2.78 Å). The two N termini are in close proximity, showing a distance of 11 Å between the Cα atoms of Ala-1. *Right panel,* packing of hydrophobic residues (Tyr-21 and Trp-26 of one monomer with Tyr-16 and Phe-28 of another) at the dimer interface.

addition, Trp-26 in each monomer stacks against Tyr-21, which, in turn, makes hydrophobic interactions with Tyr-16, Phe-28 and the Cys-2–Cys-30 disulfide of the opposing monomer. It is believed that this general ("canonical") mode of dimerization is conserved among all members of the α-defensin family, even though its functional significance remains uncertain because of the paucity of data from experimental models.

A recent systematic mutational analysis of HNP1 identified Trp-26 as the most important residue for defensin activity (23). The W26A mutation dramatically impaired not only the ability of HNP1 to kill *Staphylococcus aureus*, inhibit LF, and bind HIV-1 gp120 but also its ability to self-associate in surface plasmon resonance experiments. Although Trp-26 of HNP1 did not directly participate in the dimer interface, it stabilized it substantially. Furthermore, increased hydrophobicity of residue 26 strongly correlated to enhanced HNP1 function and self-association. In addition, a nuclear magnetic resonance study demonstrated that the HNP1 dimer disrupts lipid bilayers (24). These results suggest that HNP1 dimerization may be of functional importance under physiological conditions. However, definitive experimental evidence is still meager. To gain additional insights into the mode of action of α-defensins, we chemically constructed, structurally characterized, and functionally interrogated several monomeric and dimeric analogs of HNP1.

MATERIALS AND METHODS

Synthesis of Monomeric and Dimeric HNP1 Analogs as Follows: MeIle-20-HNP1, MeIle-20/W26A-HNP1, $(CGG\text{-}HNP1)_2$, $(CGG\text{-}W26A\text{-}HNP1)_2$, Ac-A11K-HNP1, I20A-HNP1, L25A-HNP1, and I20A/L25A HNP1—Materials used in the experiments were described elsewhere (23). The amino acid sequence of HNP1 is ^{1}ACYCRIPACIAGERRYGTCIYQGRLWAFCC^{30}. Preparation of HNP1 and W26A-HNP1, using the 2-(1*H*-benzotriazol-1-yl)-1,1,3,3-tetramethyluroniumhexafluorophosphate activation/*N*,*N*-diisopropylethylamine *in situ* neutralization protocol developed by Kent and co-workers (25) for *t*-butoxycarbonyl chemistry solid phase peptide synthesis, was previously reported (23, 26). The synthesis of MeIle-20-HNP1 and the double mutant MeIle-20/W26A-HNP1 was straightforward, involving a simple replacement of Ile-20 by its *N*-methylated form. Correct oxidative folding of the two monomeric analogs of HNP1 was achieved at 0.25 mg/ml in 25% *N*,*N*-dimethylformamide containing 2 M urea, 3 mM reduced, and 0.3 mM oxidized glutathione, pH 8.3, using the same procedures as described for wild type HNP1 (26).

HNP1 and W26A-HNP1 were extended at the N terminus by three amino acids: Cys(Acm)-Gly-Gly. Homodimerization of folded Cys(Acm)-Gly-Gly-HNP1 or Cys(Acm)-Gly-Gly-W26A-HNP1 was achieved through deprotection of Cys(Acm) and spontaneous formation of an intermolecular disulfide bond. Briefly, Cys(Acm)-Gly-Gly-HNP1 or Cys(Acm)-Gly-Gly-W26A-HNP1 was dissolved at 0.5 mg/ml in 0.1 M citric acid, 1 M HCl, to which 5 mM iodine prepared in methanol was added dropwise until a stable yellow color was observed. After 30 min, the reaction was quenched with 0.2 M ascorbic acid, and the resultant defensin dimers, $(CGG\text{-}HNP1)_2$ and $(CGG\text{-}W26A\text{-}HNP1)_2$, were subsequently purified. Because α-aminobutyric acid (Abu) is isosteric to Cys, AbuGG-HNP1 as a control for the dimer $(CGG\text{-}HNP1)_2$ was also synthesized, folded, and purified. In addition, a fluorescent HNP1 analog was prepared. Briefly, an N-terminally acetylated HNP1 analog, Ac-A11K-HNP1, was synthesized, folded, and purified and subsequently reacted through its only amino group at Lys-11 with Alexa Fluor 350 carboxylic acid succinimidyl ester as per the instructions provided by the manufacturer. The synthesis of

the Ala scanned mutants I20A, L25A, and double mutant I20A/L25A was essentially as described previously (23).

All defensin peptides were purified to homogeneity by preparative reverse phase-HPLC, and their molecular masses were ascertained by electrospray ionization mass spectrometry (ESI-MS). Defensin stock solutions prepared with water were quantified spectroscopically at 280 nm using molar extinction coefficients calculated according to the algorithm of Pace *et al.* (27).

Structural Studies of MeIle-20-HNP1 and (CGG-HNP1)$_2$—Crystals of MeIle-20-HNP1 and (CGG-HNP1)$_2$ were grown using the hanging-drop vapor diffusion method at room temperature. Initial screenings were performed either manually or robotically with the commercially available crystallization sparse matrix screens from Hampton Research. Final crystallization conditions are detailed in the supplemental material. X-ray diffraction data for MeIle-20-HNP1 and (CGG-HNP1)$_2$ were collected using synchrotron radiation at the SER-CAT sector 22 beamlines of the Advanced Photon Source (Argonne, IL) equipped with MAR225 or MAR300 CCD detectors. Data were integrated and scaled with HKL2000 (28). All structures were solved using the molecular replacement method as implemented in the program Phaser from the CCP4 suite (29). The monomer of HNP3 (Protein Data Bank code 1DFN) was used as a search model (21). The structural refinements were performed using the program Refmac (30) coupled with a manual refitting and rebuilding with the program COOT (31). The data collection and refinement statistics are summarized in supplemental Table S1. The coordinates and structure factors have been deposited in the Protein Data Bank with accession codes 3HJD and 3HJ2 for MeIle-20-HNP1 and (CGG-HNP1)$_2$, respectively. Molecular graphics were generated using the programs PyMOL and Ribbons (32).

Functional Assays—Anthrax LF was obtained from List Biological Laboratories, Inc. HIV$_{BaL}$ gp120, expressed in T-REx^{TM}-293 cells and affinity-purified, was a generous gift from Profectus Biosciences, Inc. Inhibition of LF by defensins was quantified as described (18). Briefly, freshly prepared LF at a final concentration of 1 μg/ml (~10 nM) was incubated at 37 °C for 30 min with a 2-fold dilution series of defensin in 20 mM HEPES buffer containing 1 mM $CaCl_2$ and 0.5% Nonidet P-40, pH 7.2. 20 μl of LF substrate, Ac-NleKKKKVLP-*p*-nitroanilide (where Nle is norleucine) at 1 mM in the buffer, was added to each well to a final concentration of 100 μM in a total volume of 200 μl. The enzyme activity, characterized as a time-dependent absorbance increase at 405 nm because of the release of *p*-nitroaniline, was monitored at 37 °C over a period of 5 min on a 96-well V_{max} microplate reader (Molecular Devices). Data are presented in a plot showing percent inhibition *versus* defensin concentration, from which IC_{50} values (the concentration of defensin that reduced the enzymatic activity of LF by 50%) were derived by a nonlinear regression analysis.

Surface plasmon resonance binding studies were done at 25 °C on a BIAcore T100 System (BIAcore, Inc., Piscataway, NJ). The pH 7.4 assay buffer contained 10 mM HEPES, 150 mM NaCl, 0.05% surfactant P20 ± 3 mM EDTA. LF (2500 RUs), gp120 (2830 and 3198 RUs) and HNP1 (285 RUs) were immobilized on CM5 sensor chips using standard amine-coupling chemistry, and measurements were done as described (18). Binding isotherms were analyzed with manufacturer-supplied software for BIAcore T100 and/or GraphPad Prism 4.0.

Virtual colony counting was used to quantify killing of *S. aureus* ATCC 29213 and *E. coli* ATCC 25922 as described (33). Briefly, a 2-fold dilution series of defensin, ranging from 25 to 0.195 μM in 10 mM sodium phosphate, pH 7.4, was incubated at 37 °C for 2 h with *E. coli* or *S. aureus* (1×10^6 CFU/ml), followed by addition of twice-concentrated Mueller-Hinton broth (2× MHB) and kinetic measurements of bacterial growth at 650 nm over 12 h. To increase the sensitivity of the assay, 1% tryptic soy broth was added to the 10 mM phosphate buffer, which produced 1–2 orders lower survival at a given concentration of HNP1 compared with that reported in the absence of tryptic soy broth. HNP1 is preferentially effective against bacteria that are metabolically active and growing. The addition of a 1:100 dilution of conventional tryptic soy broth to the assay buffer provides enough nutrients to allow three or four bacterial doublings, without significantly altering the overall concentrations of NaCl or divalent cations. Data analysis used a Visual Basic script to calculate the time necessary for each growth curve to reach a threshold absorbance change at 650 nm of 0.02. The virtual LD_{50} (vLD_{50}), vLD_{90}, vLD_{99}, and $vLD_{99.9}$ are defensin concentrations with survival rates of 0.5, 0.1, 0.01, and 0.001, respectively.

Fluorescence Polarization Assays—Fluorescence polarization measurements were done on a K2 spectrofluorometer (ISS, Champagne, IL) with motorized Glann-Thompson polarizers in the excitation and emission light paths. Alexa Fluor 350 was excited at 380 nm, and emission was observed at 460 nm through a bandpass filter of 40 nm. Measured fluorescence polarizations were corrected for different detection sensitivities to two orthogonal polarizations using an L-format configuration and the *G*-factor (34). Corrections for decreased fluorescence lifetimes (thus increased polarization) were made for >1 μM samples in PBS. The polarization values in PBS and HEPES were similar after correction. Defensins were prepared by 3-fold serial dilutions (from 30 to 0.01 μM) of stock solutions in PBS or 20 mM HEPES, pH 7.2. The diluted samples were allowed to equilibrate overnight before polarization measurements in a 10 × 4-mm cuvette.

RESULTS

HNP1 Dimerizes in Solution—All crystal structures of α-defensins show a conserved mode of dimerization and suggest the possibility of forming higher order oligomers (21, 22). Defensin dimerization can also be demonstrated by gel electrophoresis (Fig. 2). However, evidence of defensin dimerization under physiological conditions has been lacking. To examine this, we synthesized an *N*-acetylated, A11K analog of HNP1 and attached Alexa Fluor 350 to the ϵ-amino group of Lys-11. Alexa Fluor 350 was chosen because the small overlap between its absorption and emission spectra ensures minimal homo-energy transfer between dyes in aggregated HNP1 and thus little or no effect on polarization values. This is important because the small size of HNP1 (3.4 kDa) will bring the two dye molecules in close proximity upon dimerization. Residue 11 was selected for labeling due to its minimal interference with defen-

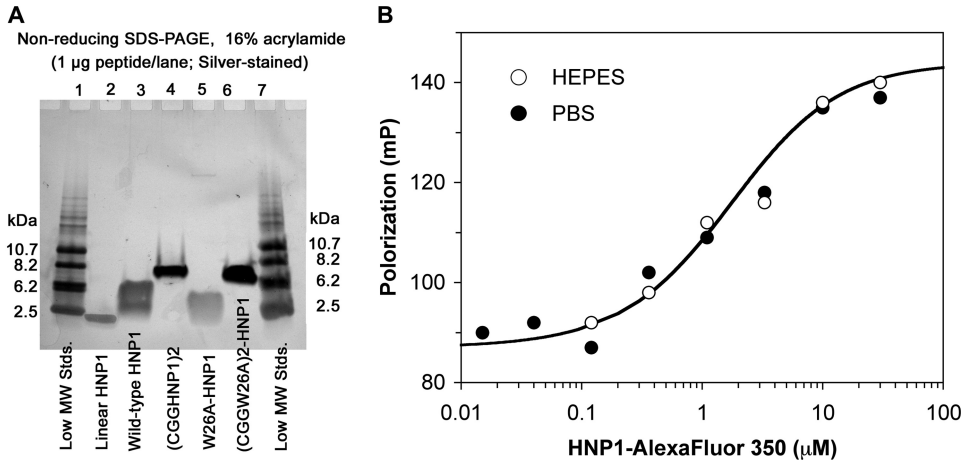

FIGURE 2. **Evidence for HNP1 dimerization.** *Left panel,* silver-stained, 16% Novex® Tricine gel (Invitrogen). The sample and running buffers, also Novex® products, contained SDS but lacked reducing agents. *Gel lanes 1* and *7* contained low molecular weight standards from Amersham Biosciences that were fragments of cyanogen-bromide-treated horse myoglobin. *Lanes 2–6* contained 1 μg each of the following defensins: *lane 2*, an HNP1 analog in which every cysteine was changed to alanine; *lane 3*, wild type HNP1; *lane 4*, $(CGG\text{-}HNP1)_2$ dimer; *lane 5*, W26A-HNP1; *lane 6*, $(CGG\text{-}W26A\text{-}HNP1)_2$ dimer. *Lanes 3* and *5*, the migration zones of monomeric wild type HNP1 and W26A-HNP1 overlapped, but W26A clearly showed less self-association, lending additional support to the evidence shown in the main text that the self-association of W26A-HNP1 was impaired. *Right panel,* concentration-dependent oligomerization of an Alexa Fluor 350-labeled HNP1 analog. Fluorescence polarization was measured at room temperature. A four-parameter logistic regression analysis was performed using the equation $Y = P_{low} + (P_{high} - P_{low})/(1 + C_0/X)^n$, which yielded $P_{low} = 87$ mP (polarization of monomers), $P_{high} = 144$ mP (polarization of dimers), $C_0 = 2.0$ μM (mid-point concentration), and $n = 0.88$ (slope). After lifetime corrections, polarization in PBS (*closed circles*) and 20 mM HEPES, pH 7.2 (*open circles*), are equal, within experimental error.

sin folding and dimerization, as judged by structural analysis of wild type HNP1 (supplemental Fig. S1).

The principles of fluorescence polarization are that monomeric HNP1 molecules tumble faster than dimers in solution, and upon excitation by polarized light, monomers "scramble" the polarization of emitted light more efficiently. Thus, dimerization causes decreased rotational rates and increased polarization of emitted light. A titration curve is generated from measurements of polarized fluorescence, and the dimerization process can be quantitatively evaluated based on known mathematical models (34). We measured concentration-dependent fluorescence polarization (Fig. 2). The polarization value was roughly 87 millipolarization units for monomers and 144 millipolarization units for dimers, in agreement with polarization models for labeled biomolecules of about 3 kDa (34). Dimerization of Ac-A11K-HNP1 occurred at concentrations above ~100 nM, reached a mid-point at 2 μM, and plateaued above ~10 μM. As the total concentration of HNP1–3 in a neutrophil's azurophilic granules is about 15 mM (35), human neutrophil peptide likely form dimers and possibly higher order oligomers within phagocytic vacuoles.

De Novo Designed Monomeric and Dimeric Analogs and Structural Validation—To assess the functional implications of HNP1 dimerization, we designed two dimerization-impaired HNP1 analogs (MeIle-20-HNP1 and MeIle-20/W26A-HNP1), and two obligate defensin dimers $(CGG\text{-}HNP1)_2$ and $(CGG\text{-}W26A\text{-}HNP1)_2$. The dimer interface of HNP1 is stabilized by four backbone-backbone H-bonds formed between Ile-20 and Thr-18 (Fig. 1). Such backbone H-bonding typically contributes about −1.5 kcal/mol to the binding free energy for protein-protein interactions (36). Methylating the peptide bond between Cys-19 and Ile-20 of HNP1 (from –CONH- to $-CON(CH_3)-$) removes the two backbone H-bonds donated by Ile-20 and adds two methyl groups at the dimer interface, thereby imparting steric and energetic impediments to stable dimer formation. Similar chemical modifications were used to disrupt the quaternary structure of a chemokine without impacting its three-dimensional fold (37).

In the dimer structure of HNP1, the N termini of the two monomers are in close proximity. Consequently, tethering these N termini via a disulfide bond should create a constitutive dimer with little structural perturbation to the monomers. To ensure that the extra S–S bond did not introduce conformational constraints that would destabilize the dimer interface, we interposed two additional Gly residues between Cys and the N terminus of HNP1.

The crystal structures of MeIle-20-HNP1 and $(CGG\text{-}HNP1)_2$ were determined at 1.65 and 1.40 Å, respectively. At the tertiary structure level, both mutants are very similar to wild type HNP1 (Fig. 3). The root mean square (r.m.s.) deviations calculated for equivalent main-chain atoms of either mutant and the wild type defensin approximate 0.4–0.5 Å. However, MeIle-20-HNP1 does not form definite oligomers in the crystal, and both monomers residing in the asymmetric unit participate in very different crystal contacts. By contrast, two HNP1 units tethered by the N-terminal linker in $(CGG\text{-}HNP1)_2$ associate into a dimer that has the topology typical for α-defensins (Fig. 3). Significantly, changes introduced to both mutants (*i.e.* the *N*-methylation in MeIle-20-HNP1 and the N-terminal extension in the covalent dimer) are well defined by a corresponding electron density (supplemental Fig. S2). Detailed analysis of MeIle-20-HNP1 indicates that the side chains of almost all residues have conformations identical to their equivalents in the wild type defensin. The only exceptions are Arg-15, Tyr-21, and Arg-24. Reorientation of the side chain of Tyr-21 is likely related to different oligomeric states of MeIle-20-HNP1 and wild type HNP1, because in the dimer this residue interacts with atoms from the opposing monomer. The r.m.s. deviations

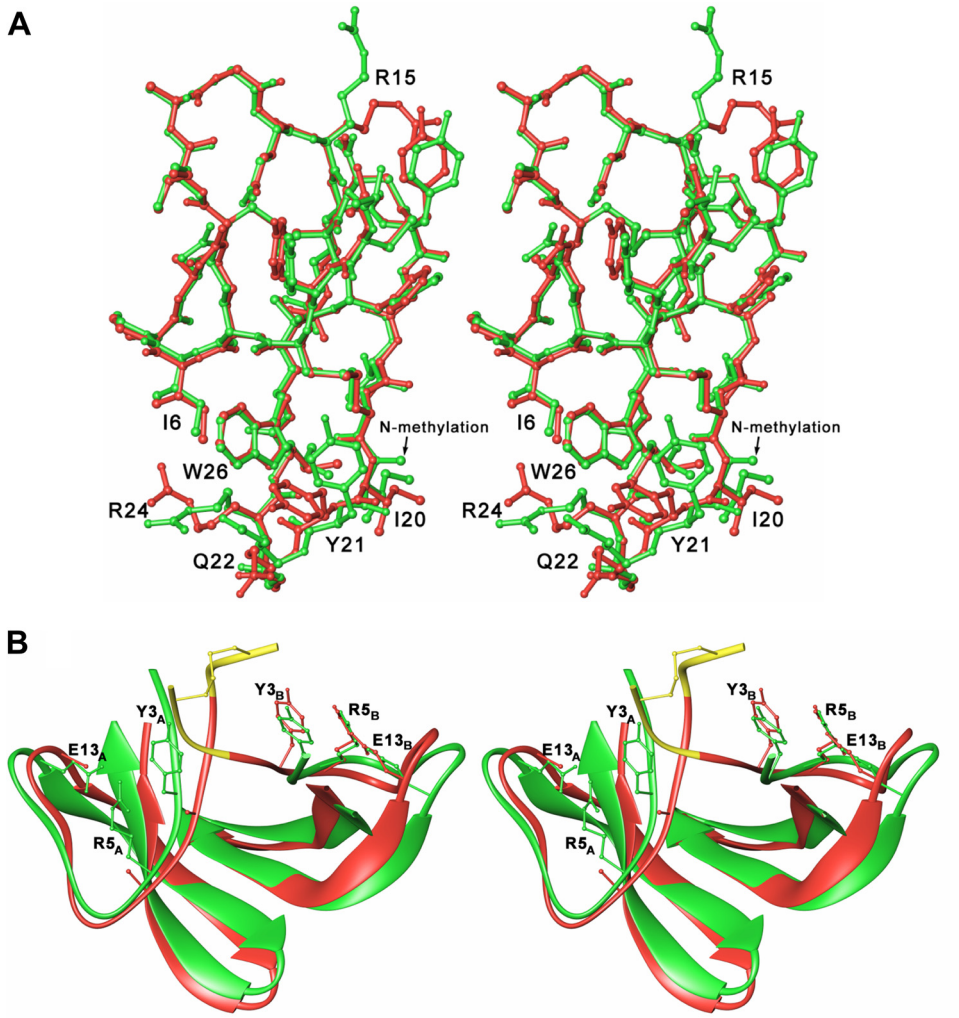

FIGURE 3. **Crystal structures of monomeric and dimeric HNP1.** *A,* stereo view of superimposed monomers of MeIle-20-HNP1 (*green*) and wild type HNP1 (*red*) with labeled side chains of residues accommodating different conformations in the two proteins. The *N*-methylation of Ile-20 is also shown. *B,* stereo view of superimposed $(CGG\text{-}HNP1)_2$ (*red*) and dimeric HNP1 (*green*). The $(CGG)_2$-linker is *yellow*. In the *A* chain of $(CGG\text{-}HNP1)_2$, the side chains (not shown) of Tyr-3, Arg-5, and Glu-13 are disordered. It is evident that the standard conformation of Tyr-3^A is structurally incompatible with the $(CGG)_2$-linker.

of the side chain atoms of the Arg-15 and Arg-24 residues are far higher than the other residues of MeIle-20-HNP1 but not $(CGG\text{-}HNP1)_2$, indicating that dimerization and/or crystal packing may destabilize these arginine side chains. Somewhat more significant, conformational differences are seen between $(CGG\text{-}HNP1)_2$ and wild type HNP1. Half of the mutant, corresponding to one defensin monomer, is structurally nearly identical to the native defensin (chain B in Fig. 3). However, in the second half (chain A), the electron density is completely missing for the side chains of Arg-5, and Glu-13 (which form a salt bridge conserved in nearly all vertebrate defensins) and Tyr-3, suggesting their disorder. Further analysis indicates that the $(CGG)_2$ linker in $(CGG\text{-}HNP1)_2$ forces a displacement of the Tyr-3 side chain from its standard position to the site of the Arg-5···Glu-13 salt bridge, causing all three side chains to become structurally labile. Overall, the crystal structures of MeIle-20-HNP1 and $(CGG\text{-}HNP1)_2$ validated the design of dimerization-impaired monomers and constitutive dimers of HNP1.

HNP1 dimerization contributes to its killing of S. aureus—HNP1 kills Gram-positive bacteria much more effectively than Gram-negative strains (18, 33). Fig. 4 and Table 1 show the bactericidal activities of HNP1, AbuGG-HNP1, MeIle-20-HNP1, and $(CGG\text{-}HNP1)_2$ against *S. aureus* and *E. coli*. AbuGG-HNP1 and wild type HNP1 killed *S. aureus* similarly. *S. aureus* behaved differently toward the obligate HNP1 monomer and constitutive HNP1 dimer. At 12.5 μM, wild type HNP1 reduced *S. aureus* survival by 5 logs and exterminated it at 25 μM. In contrast, 50 μM MeIle-20-HNP1 reduced *S. aureus* survival by <2 logs. From their vLD_{99} and $vLD_{99.9}$ values, *N*-methylation of Ile-20 weakened HNP1 killing of the bacterium by at least 1 order of magnitude. Interestingly, covalent tethering of HNP1 improved its bactericidal activity by ~3-fold compared with AbuGG-HNP1. Enhancement of *S. aureus* killing by the obligate dimer was modest, presumably because AbuGG-HNP1 can itself dimerize. In a separate vCC assay, however, both $(CGG\text{-}W26A\text{-}HNP1)_2$ and W26A-HNP1 were ineffective against *S. aureus*. Thus, covalent tethering failed to make W26A-HNP1 competent for killing this bacterium. Overall, these data show that canonical dimerization of wild type HNP1 contributes to its bactericidal activity against *S. aureus* and confirm the critical enabling role of the Trp-26 residue in this process.

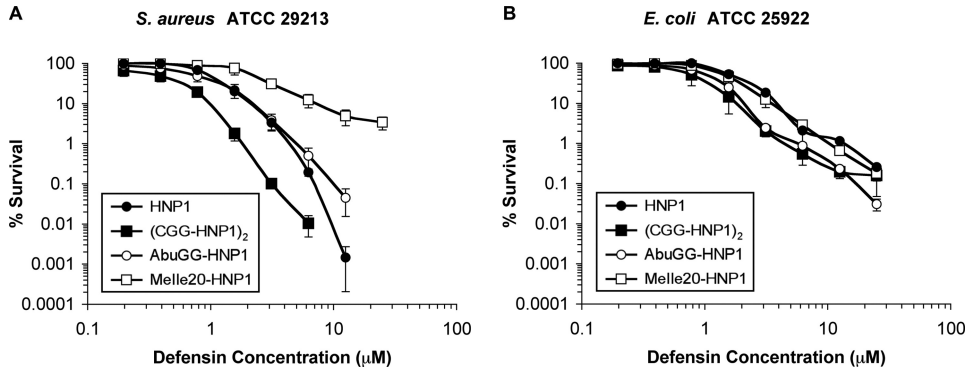

FIGURE 4. **Bactericidal activity of native and modified α-defensins (0.2 to 25 μM) against *S. aureus* (*left panel*) and *E. coli* (*right panel*), determined by virtual colony counting.** *Filled markers* are HNP1 (●) and $(CGG\text{-}HNP2)_2$ (■); *open markers* represent AbuGG-HNP1 (○) and MeIle-20-HNP1 (□). Means ± S.D. ($n = 3$) are shown. Media contained 1% tryptic soy broth. No results are shown for 12.5 and 25 μM $(CGG\text{-}HNP1)_2$ because the peptide formed precipitates. Points scored as zero survival were not plotted.

TABLE 1

Antimicrobial virtual lethal doses (vLD, μM) that kill 50, 90, 99, and 99.9% of *E. coli* and *S. aureus* input viable cells, as inferred using the virtual colony counting (vCC) procedure

The data were obtained from three independent assays (means ± S.E.).

Defensin	*E. coli* ATCC 25922				*S. aureus* ATCC 29213			
	vLD_{50}	vLD_{90}	vLD_{99}	$vLD_{99.9}$	vLD_{50}	vLD_{90}	vLD_{99}	$vLD_{99.9}$
HNP1	1.7 ± 0.0	4.5 ± 0.2	14.0 ± 1.1	> 50	1.0 ± 0.1	2.4 ± 0.2	5.1 ± 0.5	8.7 ± 0.7
AbuGG-HNP1	1.0 ± 0.2	2.4 ± 0.2	5.9 ± 0.5	19.6 ± 1.3	0.7 ± 0.3	2.3 ± 0.4	5.4 ± 0.7	10.8 ± 1.4
MeIle-20-HNP1	3.2 ± 1.3	5.2 ± 0.7	11.0 ± 0.9	34.6 ± 6.5	3.6 ± 0.9	8.1 ± 2.0	> 50	> 50
$(CGG\text{-}HNP1)_2$	0.8 ± 0.3	1.9 ± 0.6	5.0 ± 0.9	16.4 ± 0.0	0.5 ± 0.0	1.1 ± 0.1	2.1 ± 0.3	3.4 ± 0.3

In contrast, very different results were obtained with *E. coli*. As shown in Fig. 4*B* and Table 1, the control analog AbuGG-HNP1 was 2–3-fold more effective than HNP1 in killing *E. coli*. However, MeIle-20-HNP1 and $(CGG\text{-}HNP1)_2$ showed bactericidal activity that was nearly identical to their respective controls, HNP1 and AbuGG-HNP1, suggesting that HNP1-mediated killing of *E. coli* is dimerization-independent.

Dimerization Is Important for HNP1 to Inhibit LF and Bind gp120—HNP1 noncompetitively inhibits the enzymatic activity of LF with an IC_{50} of 148 nM (18) and binds HIV gp120 at nanomolar affinity (38). To examine the functional role of HNP1 dimerization, we quantified inhibition of LF activity by MeIle-20-HNP1, MeIle-20/W26A-HNP1, $(CGG\text{-}HNP1)_2$, and $(CGG\text{-}W26A\text{-}HNP1)_2$ and compared their gp120 binding properties using surface plasmon resonance. Table 2 contains IC_{50} concentrations for LF inhibition, and Fig. 5*A* shows these results graphically. Binding kinetics of the defensins on immobilized gp120 are shown in Fig. 5*B*. Wild type HNP1, W26A-HNP1, and the control analog AbuGG-HNP1 were used for comparison.

As AbuGG-HNP1 (IC_{50} = 98 nM) and HNP1 had similar inhibitory activity, extending the N terminus of HNP1 by three residues was functionally inconsequential. In contrast, *N*-methylating Ile-20 greatly reduced the ability of HNP1 to inhibit LF activity, as evidenced by an 11-fold increase in IC_{50} to 1.6 μM. Although very significant, this impairment is only about half of the 20-fold IC_{50} change caused by the W26A mutation (23). HNP1 containing both mutations (MeIle-20-W26A-HNP1) had an IC_{50} of 42 μM, almost 300-fold higher than wild type HNP1. Clearly, the W26A and MeIle-20 mutations are synergistic in their effect on LF inhibition. Importantly, $(CGG\text{-}W26A\text{-}HNP1)_2$ showed an IC_{50} value (151 nM) nearly identical to that of wild type HNP1, suggesting that covalent tethering restored the ability of W26A-HNP1 to inhibit LF. Covalent tethering did not improve the inhibitory activity of wild type HNP1, consistent with its ability to dimerize spontaneously.

TABLE 2

IC_{50} values of $(CGG\text{-}HNP1)_2$, $(CGG\text{-}W26A\text{-}HNP1)_2$, MeIle-20-HNP1, MeIle-20/W26A-HNP1, and AbuGG-HNP1 for lethal factor determined by enzyme inhibition kinetics at 37 °C in 20 mM HEPES buffer containing 1 mM $CaCl_2$ and 0.5% Nonidet P-40, pH 7.2

The data are averages of three independent measurements (means ± S.E.). The previously reported IC_{50} values of the wild type defensin and W26A-HNP1 were determined in the same assays (23).

Defensin	IC_{50}	Defensin	IC_{50}
	nM		nM
Wild type HNP1	148 ± 11	W26A-HNP1	2786 ± 396
AbuGG-HNP1	98 ± 11	MeIle-20/W26A-HNP1	41755 ± 3831
MeIle-20-HNP1	1592 ± 157	$(CGG\text{-}W26A\text{-}HNP1)_2$	151 ± 18
$(CGG\text{-}HNP1)_2$	70 ± 7		

Concordant results were obtained with the defensins binding to HIV gp120. Their relative effectiveness was as follows: HNP1 ≈ $(CGG\text{-}HNP1)_2$ > $(CGG\text{-}W26A\text{-}HNP1)_2$ > MeIle-20-HNP1 ≈ W26A-HNP1 ≫ MeIle-20/W26A-HNP1. As shown in Fig. 5*B*, although the N-terminal tethering improved W26A-HNP1 binding to gp120, it had little impact on the wild type defensin. *N*-Methylation of Ile-20 or the W26A mutation significantly impaired the ability of HNP1 to bind gp120, whereas their combination fully incapacitated it. Taken together, the LF inhibition and HIV gp120 binding data demonstrate the functional importance of HNP1 dimerization.

Alternative Modes of Self-association Exist—HNP1 not only binds to bacterial and viral proteins, it also displays a strong tendency to self-associate. How does self-association occur between solution phase and immobilized defensin molecules?

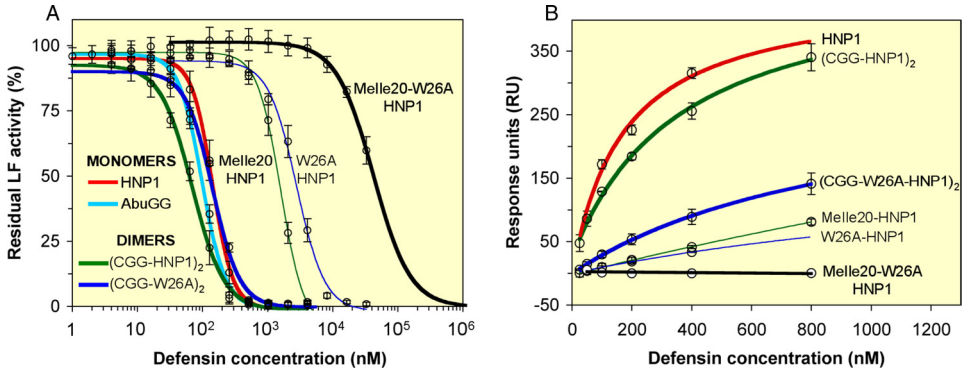

FIGURE 5. **Defensin inhibition of anthrax LF and binding to HIV-1 gp120.** *A,* dose-dependent inhibition of anthrax LF activity by selected defensin analogs. The symbols show values (mean ± S.D.) from three independent kinetic assays at 37 °C. *B,* binding of selected defensins to immobilized HIV-1 gp120 (2830 RUs) after 300 s at room temperature ($n = 3$).

To answer this question, we compared the ability of wild type HNP1, W26A-HNP1, $(CGG\text{-}HNP1)_2$, and $(CGG\text{-}W26A\text{-}HNP1)_2$ in solution to bind to HNP1, W26A-HNP1, or MeIle-20-HNP1 that had been immobilized. Because RU are proportional to the mass added to the biosensor, it is possible to estimate the "molar ratio" (19), *i.e.* the average number of solution phase HNP1 molecules bound per immobilized HNP1 "receptor." As shown in Fig. 6, the W26A mutation greatly diminished the ability of HNP1 or N-terminally tethered HNP1 to self-associate on all surfaces, consistent with the important role of Trp-26 in HNP1 dimerization and further self-association. Covalent tethering significantly enhanced further self-association of wild type HNP1 at concentrations greater than 2.5 μM, but it failed to rescue W26A-HNP1, suggesting that Trp-26 is important for mediating the further self-association (*i.e.* assembly) of canonical HNP1 dimers. Remarkably, binding of solution phase HNP1 was independent of the MeIle-20 or W26A mutation of the immobilized defensin, thereby excluding canonical dimerization as the mode of further self-association/assembly between solution phase and immobilized defensin molecules.

Despite the critical role of Trp-26 in mediating HNP1 dimerization and subsequent self-association, the W26A mutation did not completely eliminate the process, suggesting that alternative modes of self-association may exist. Structural analysis of wild type HNP1 and many HNP1 analogs shows that two canonical HNP1 dimers can be brought together to form a tetramer by extensive hydrophobic interactions involving the side chains of four pairs of Ile-20 and Leu-25 (Fig. 7*A*). Analysis of wild type HNP1 by the PISA (Protein Interfaces, Surfaces and Assemblies) interactive tool yields a buried surface area of 2280 Å^2 at the dimer-dimer interface and a calculated dissociation free energy of 2.2 kcal/mol. To experimentally probe this possible mode of self-association, we examined the ability of I20A-HNP1, L25A-HNP1. and the double mutant I20A/L25A-HNP1 to self-associate at different concentrations (from 125 nM to 8 μM) to immobilized HNP1. Wild type HNP1 was used as a control. As shown in Fig. 7, *B–D*, both the I20A and the L25A mutations weakened HNP1 self-association with the latter being more deleterious than the former. As expected, the I20A/L25A-HNP1 double mutant displayed the least amount of binding to immobilized HNP1, ~3-fold less than the wild type defensin. These results suggest that Ile-20 and Leu-25 may also play a role in mediating HNP1 oligomerization on the surface of target proteins such as LF and gp120. Alternative modes of HNP1 oligomerization may provide additional molecular diversity at the quaternary structural level that imparts HNP1 functional versatility, as suggested previously (18).

DISCUSSION

Specific association of protein subunits to form dimers and higher order oligomers has functional ramifications. For example, allosteric regulation of protein function can be achieved through changes in protein quaternary structure induced by regulatory molecules (39, 40); DNA transcription initiated by cooperative protein binding often necessitates oligomerization of transcription factors to ensure high affinity and specificity (40, 41). To this end, x-ray crystallography has played a powerful role in elucidating the structural basis of function of multimeric proteins in a great variety of biological processes. A caveat is that weak and nonspecific interactions between protein molecules can also occur, particularly at high concentrations, in regions that are not part of a functional interface, as often illustrated by the molecular contacts within crystals (40). Thus, the multimeric crystal structure of a protein does not always confer functional significance to features of its quaternary assembly because of "crystal packing." A well studied example is provided by chemokines, which crystallize as homodimers and/or higher order homo-oligomers but function as monomers (37, 42). By coupling protein backbone engineering to structural and functional analysis, we have unequivocally demonstrated that the canonical mode of dimerization of HNP1 is important with respect to its ability to kill *S. aureus*, inhibit LF, and bind HIV gp120.

The sequences of HNP1 and -3 are identical except that the N-terminal residue is alanine in the former and aspartic acid in the latter. When the dimeric HNP3 crystal structure was reported in 1991 (21), the authors noted the 344-Å^2 solvent-accessible patch formed by the hydrophobic side chains of Tyr-16, Tyr-21, Trp-26, and Phe-28. They speculated that defensin dimers might permeabilize microbial membranes in three ways as follows: a wedge hypothesis, a dimer-pore hypothesis, and a general pore hypothesis. From modeling studies, they concluded that a minimum of four dimers would be needed to

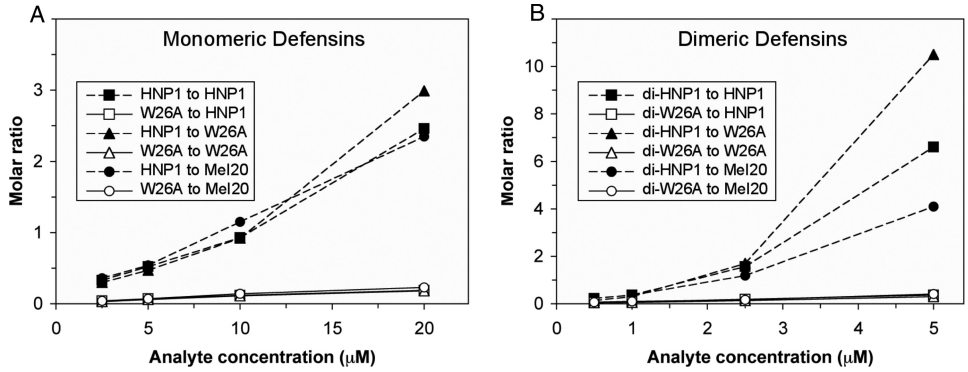

FIGURE 6. **Self-association of HNP1 and HNP1 analogs as determined by surface plasmon resonance techniques.** *A,* binding of monomeric HNP1 and HNP1 analogs to immobilized HNP1, W26A-HNP1, and Melle-20-HNP1 defensins. *B,* binding of selected defensin dimers to the same immobilized defensins.

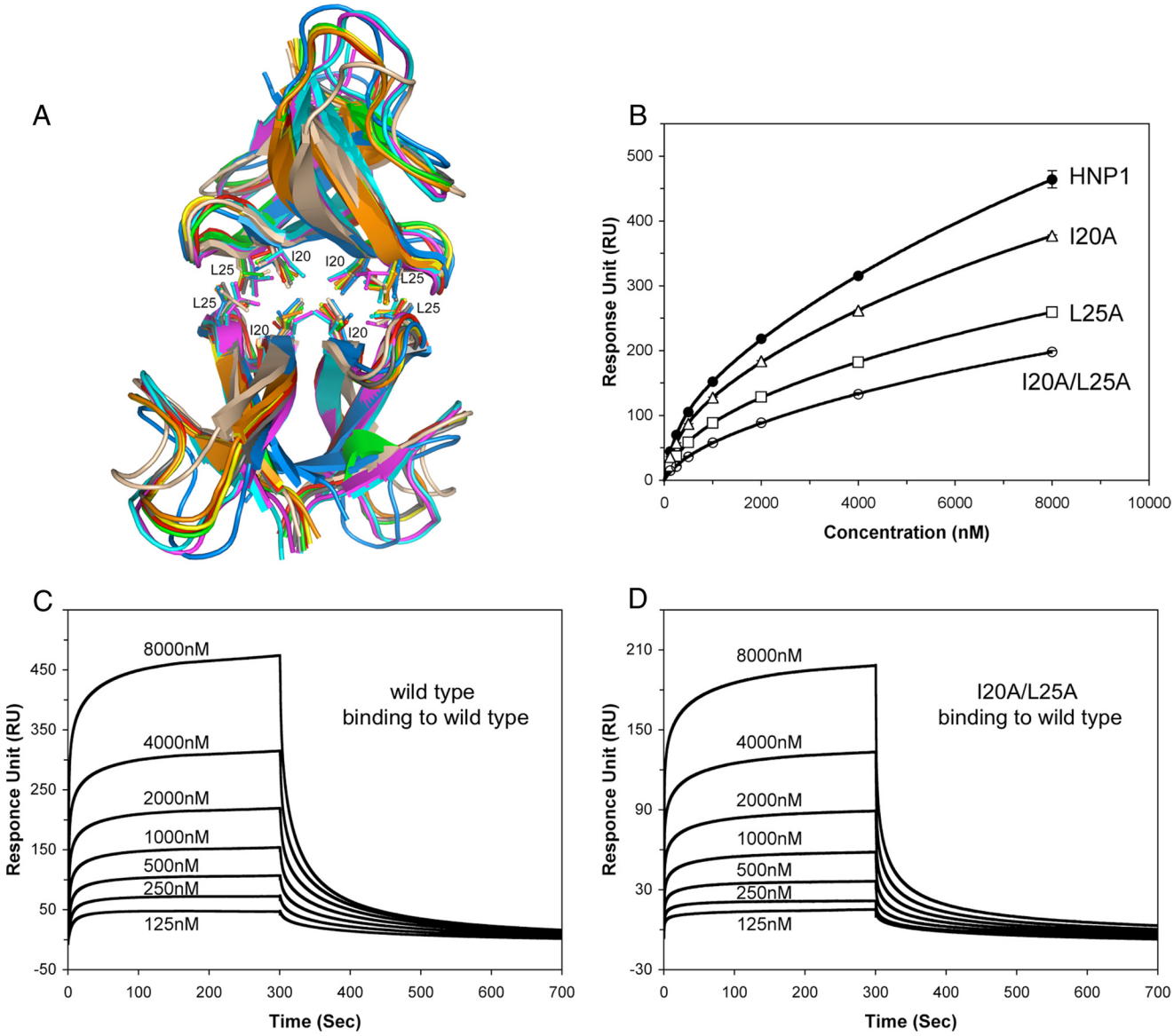

FIGURE 7. **Possible mode of HNP1 tetramerization.** *A,* mode of tetramerization of HNP1 and Y3A-, Y16A-, Y21A-, Q22A-, R24A-, W26Abu-, W26α-aminoheptanoic acid-, and F28A-HNP1. *B,* binding (characterized by RU values at 300 s of association) of HNP1, I20A-HNP1, L25A-HNP1, and I20A/L25A-HNP1 to 285 RUs of immobilized HNP1 as a function of concentration. The RU values (mean ± S.D.) are from three separate experiments performed at room temperature. *C,* representative isotherms of the self-association of HNP1. *D,* representative isotherms of the association of I20A/L25A-HNP1 to HNP1.

complete a pore. In all these models, the canonical HNP1 dimer was implicated as a functional quaternary structure minimally required for membrane permeabilization. Our results on HNP1 support a role for defensin dimerization in *S. aureus* killing, although they do not speak directly to pore formation *versus* inhibition of lipid II (44) as the operant mechanism. In contrast,

because *E. coli* killing by HNP1 was independent of its dimerization, nondimer pore forming mechanisms also exist.

A currently prevailing view postulates that α-defensins kill bacteria such as *E. coli* by forming pores or functionally equivalent defects in microbial membranes. Such lesions dissipate the proton-motive force, cause leakage of intracellular contents, prevent accumulation of external nutrients, and make intracellular targets accessible (13, 14, 43). From a forensic perspective, disruption of membrane integrity is obligatory, even if the ultimate coup de grace is administered by a downstream event. More recent evidence suggests that HNP1 kills *E. coli* by a process that is mechanistically distinct from its action that kills *S. aureus* (18). First, although the cationicity of HNP1 dictates its bactericidal activity against *E. coli*, the hydrophobicity of HNP1 is the most critical molecular determinant for its ability to kill *S. aureus* (23). Second, HNP1 killing of *E. coli* is independent of its tertiary structure, whereas the loss of disulfide bonding inactivates the peptide against *S. aureus* (18). Similar results were also found for HD5 (44). Third, although the L- and D-enantiomers of HNP1 or HD5 display identical bactericidal activities against the Gram-negative bacterium, *E. coli*, L-HNP1, and L-HD5 are significantly more active than their D-enantiomers in killing the Gram-positive strain, *S. aureus* (18). The disparity in bactericidal activity against *S. aureus* between L- and D-defensins suggests that α-defensin-mediated membrane disruption may not be the sole molecular event leading to the demise of *S. aureus* (18). In fact, HNP1 can also interact with other molecular targets such as lipid II to inhibit bacterial cell wall synthesis preferentially in *S. aureus* (45), a mode of action reminiscent of the lantibiotic peptide nisin (46, 47) and other defensins (48–50). Our latest finding that *N*-methylation of Ile-20 or covalent tethering had, at most, minor effects on the bactericidal activity of HNP1 against *E. coli* provides additional evidence that different mechanisms underlie the HNP1-mediated killing of *E. coli* and *S. aureus*.

Regardless of the mode(s) of action of HNP1, dimerization is likely to enhance its binding to a great variety of molecular targets, as diverse as LF and HIV gp120. The presence of a large hydrophobic patch comprising Tyr-16, Tyr-21, Trp-26, and Phe-28 at the dimer interface may play a major role in this regard. Of these four aromatic residues, Trp-26 is particularly important (23), because it plays a prominent role in structurally stabilizing the canonical HNP1 dimer interface and in mediating direct interactions of HNP1 with target molecules.

How exactly does Trp-26 promote HNP1 self-association? Answers to this question are pertinent to a better understanding of how α-defensins interact with and oligomerize on the surface of target molecules (19, 51). We previously demonstrated that Trp-26 was critical for the self-association of submicromolar concentrations of HNP1 to surface-immobilized HNP1 (23). The present fluorescence polarization studies establish that HNP1 dimerizes in solution at a mid-point concentration of ~2 μM. Thus, at sub-micromolar concentrations Trp-26 must mediate the self-association of HNP1 monomers instead of canonical dimers, although the subsequent canonical dimerization of surface-bound HNP1 monomers cannot be ruled out. This raises the intriguing possibility that Trp-26 may interact directly with LF and gp120 at concentrations where HNP1 exists as a monomer. The functional data on LF inhibition and gp120 binding are consistent with this inference because the W26A and MeIle-20 mutations were synergistic in their effects, whereas *N*-methylation of Ile-20 alone substantially impaired the ability of HNP1 to dimerize. Trp-26 may therefore contribute to HNP1 function independently by mediating direct "nonspecific" interactions between monomeric HNP1 and target (glyco)protein and (glyco)lipid molecules. A logical extension from this line of reasoning is that at high concentrations Trp-26 will also mediate the association of canonical HNP1 dimers to LF and gp120. Because the dimer is an intermediate in the formation of higher order oligomers, the dimeric mode of interaction is likely to be important due to the effect of multivalency. It is conceivable that a general feature of the activity of HNP1 is the Trp-26-mediated binding of HNP1 monomers and canonical dimers to a variety of molecular, bacterial, and viral targets. Finally, it is worth pointing out that the functional importance of the dimerization of HNP1 is conceptually different from the observations made by others that covalently linking two cationic peptides enhances bacterial killing in a structure-independent manner due to increased cationic charge density (52, 53). Our covalently tethered HNP1 dimer $(CGG\text{-}HNP1)_2$ was similarly active to its untethered control (AbuGG-HNP1) with respect to LF inhibition, gp120 binding, and bacterial killing, suggesting that AbuGG-HNP1, like wild type HNP1, is already dimerized during its action.

Acknowledgments—We thank the X-ray Crystallography Core Facility of the University of Maryland at Baltimore for providing crystallographic equipment and resources. Use of the Advanced Photon Source was supported by the United States Department of Energy, Offices of Science and of Basic Energy Sciences, under Contract W-31-109-Eng38.

REFERENCES

1. Bevins, C. L. (2006) Paneth cell defensins: key effector molecules of innate immunity. *Biochem. Soc. Trans.* **34,** 263–266
2. Ganz, T. (2003) Defensins: antimicrobial peptides of innate immunity. *Nat. Rev. Immunol.* **3,** 710–720
3. Lehrer, R. I. (2004) Primate defensins. *Nat. Rev. Microbiol.* **2,** 727–738
4. Selsted, M. E., and Ouellette, A. J. (2005) Mammalian defensins in the antimicrobial immune response. *Nat. Immunol.* **6,** 551–557
5. Zasloff, M. (2002) Antimicrobial peptides of multicellular organisms. *Nature* **415,** 389–395
6. Lehrer, R. I., and Lu, W. (2012) α-Defensins in human innate immunity. *Immunol. Rev.* **245,** 84–112
7. Ganz, T., Selsted, M. E., Szklarek, D., Harwig, S. S., Daher, K., Bainton, D. F., and Lehrer, R. I. (1985) Defensins. Natural peptide antibiotics of human neutrophils. *J. Clin. Invest.* **76,** 1427–1435
8. Selsted, M. E., Harwig, S. S., Ganz, T., Schilling, J. W., and Lehrer, R. I. (1985) Primary structures of three human neutrophil defensins. *J. Clin. Invest.* **76,** 1436–1439
9. Gabay, J. E., Scott, R. W., Campanelli, D., Griffith, J., Wilde, C., Marra, M. N., Seeger, M., and Nathan, C. F. (1989) Antibiotic proteins of human polymorphonuclear leukocytes. *Proc. Natl. Acad. Sci. U.S.A.* **86,** 5610–5614
10. Wilde, C. G., Griffith, J. E., Marra, M. N., Snable, J. L., and Scott, R. W. (1989) Purification and characterization of human neutrophil peptide 4, a novel member of the defensin family. *J. Biol. Chem.* **264,** 11200–11203
11. Jones, D. E., and Bevins, C. L. (1992) Paneth cells of the human small intestine express an antimicrobial peptide gene. *J. Biol. Chem.* **267,**

23216–23225
12. Jones, D. E., and Bevins, C. L. (1993) Defensin-6 mRNA in human Paneth cells. Implications for antimicrobial peptides in host defense of the human bowel. *FEBS Lett.* **315,** 187–192
13. Kagan, B. L., Selsted, M. E., Ganz, T., and Lehrer, R. I. (1990) Antimicrobial defensin peptides form voltage-dependent ion-permeable channels in planar lipid bilayer membranes. *Proc. Natl. Acad. Sci. U.S.A.* **87,** 210–214
14. Lehrer, R. I., Barton, A., Daher, K. A., Harwig, S. S., Ganz, T., and Selsted, M. E. (1989) Interaction of human defensins with *Escherichia coli*. Mechanism of bactericidal activity. *J. Clin. Invest.* **84,** 553–561
15. Klotman, M. E., and Chang, T. L. (2006) Defensins in innate antiviral immunity. *Nat. Rev. Immunol*. **6,** 447–456
16. Kim, C., Gajendran, N., Mittrücker, H. W., Weiwad, M., Song, Y. H., Hurwitz, R., Wilmanns, M., Fischer, G., and Kaufmann, S. H. (2005) Human α-defensins neutralize anthrax lethal toxin and protect against its fatal consequences. *Proc. Natl. Acad. Sci. U.S.A.* **102,** 4830–4835
17. Lehrer, R. I., Jung, G., Ruchala, P., Wang, W., Micewicz, E. D., Waring, A. J., Gillespie, E. J., Bradley, K. A., Ratner, A. J., Rest, R. F., and Lu, W. (2009) Human alpha-defensins inhibit hemolysis mediated by cholesterol-dependent cytolysins. *Infect. Immun*. **77,** 4028–4040
18. Wei, G., de Leeuw, E., Pazgier, M., Yuan, W., Zou, G., Wang, J., Ericksen, B., Lu, W. Y., Lehrer, R. I., and Lu, W. (2009) Through the looking glass, mechanistic insights from enantiomeric human defensins. *J. Biol. Chem.* **284,** 29180–29192
19. Lehrer, R. I., Jung, G., Ruchala, P., Andre, S., Gabius, H. J., and Lu, W. (2009) Multivalent binding of carbohydrates by the human α-defensin, HD5. *J. Immunol.* **183,** 480–490
20. Yang, D., Liu, Z. H., Tewary, P., Chen, Q., de la Rosa, G., and Oppenheim, J. J. (2007) *Curr. Pharm. Des*. **13,** 3131–3139
21. Hill, C. P., Yee, J., Selsted, M. E., and Eisenberg, D. (1991) Crystal structure of defensin HNP-3, an amphiphilic dimer. Mechanisms of membrane permeabilization. *Science* **251,** 1481–1485
22. Szyk, A., Wu, Z., Tucker, K., Yang, D., Lu, W., and Lubkowski, J. (2006) Crystal structures of human α-defensins HNP4, HD5, and HD6. *Protein Sci.* **15,** 2749–2760
23. Wei, G., Pazgier, M., de Leeuw, E., Rajabi, M., Li, J., Zou, G., Jung, G., Yuan, W., Lu, W. Y., Lehrer, R. I., and Lu, W. (2010) Trp-26 imparts functional versatility to human α-defensin HNP1. *J. Biol. Chem.* **285,** 16275–16285
24. Zhang, Y., Lu, W., and Hong, M. (2010) The membrane-bound structure and topology of a human α-defensin indicate a dimer pore mechanism for membrane disruption. *Biochemistry* **49,** 9770–9782
25. Schnölzer, M., Alewood, P., Jones, A., Alewood, D., and Kent, S. B. (1992) *In situ* neutralization in Boc-chemistry solid phase peptide synthesis. Rapid, high yield assembly of difficult sequences. *Int. J. Pept. Protein Res.* **40,** 180–193
26. Wu, Z., Powell, R., and Lu, W. (2003) Productive folding of human neutrophil alpha-defensins *in vitro* without the pro-peptide. *J. Am. Chem. Soc*. **125,** 2402–2403
27. Pace, C. N., Vajdos, F., Fee, L., Grimsley, G., and Gray, T. (1995) How to measure and predict the molar absorption coefficient of a protein. *Protein Sci*. **4,** 2411–2423
28. Otwinowski, Z., and Minor, W. (1997) Processing of X-ray diffraction data collected in oscillation mode. *Methods Enzymol.* **276,** 307–326
29. Storoni, L. C., McCoy, A. J., and Read, R. J. (2004) Likelihood-enhanced fast rotation functions. *Acta Crystallogr. D Biol. Crystallogr.* **60,** 432–438
30. Murshudov, G. N., Vagin, A. A., and Dodson, E. J. (1997) Refinement of macromolecular structures by the maximum-likelihood method. *Acta Crystallogr. D Biol. Crystallogr.* **53,** 240–255
31. Emsley, P., and Cowtan, K. (2004) Coot. Model-building tools for molecular graphics. *Acta Crystallogr. D Biol. Crystallogr.* **60,** 2126–2132
32. Carson, M. (1991) RIBBONS 2.0. *J. Appl. Crystallogr.* **24,** 958–961
33. Ericksen, B., Wu, Z., Lu, W., and Lehrer, R. I. (2005) Antibacterial activity and specificity of the six human α-defensins. *Antimicrob. Agents Chemother.* **49,** 269–275
34. Lakowicz, J. R. (2006) *Principles of Fluorescence Spectroscopy*, 3rd Ed., pp. 353–380, Springer Science, New York
35. Ganz, T., Selsted, M. E., and Lehrer, R. I. (1986) Antimicrobial activity of phagocyte granule proteins. *Semin. Respir Infect.* **1,** 107–117
36. Lu, W., Qasim, M. A., Laskowski, M., Jr., and Kent, S. B. (1997) Probing intermolecular main chain hydrogen bonding in serine proteinase-protein inhibitor complexes. Chemical synthesis of backbone-engineered turkey ovomucoid third domain. *Biochemistry* **36,** 673–679
37. Rajarathnam, K., Sykes, B. D., Kay, C. M., Dewald, B., Geiser, T., Baggiolini, M., and Clark-Lewis, I. (1994) Neutrophil activation by monomeric interleukin-8. *Science* **264,** 90–92
38. Wang, W., Owen, S. M., Rudolph, D. L., Cole, A. M., Hong, T., Waring, A. J., Lal, R. B., and Lehrer, R. I. (2004) Activity of α- and θ-defensins against primary isolates of HIV-1. *J. Immunol.* **173,** 515–520
39. Monod, J., Changeux, J. P., and Jacob, F. (1963) Allosteric proteins and cellular control systems. *J. Mol. Biol.* **6,** 306–329
40. Kuriyan, J., and Eisenberg, D. (2007) The origin of protein interactions and allostery in colocalization. *Nature* **450,** 983–990
41. Pabo, C. O., and Sauer, R. T. (1992) Transcription factors. Structural families and principles of DNA recognition. *Annu. Rev. Biochem.* **61,** 1053–1095
42. Allen, S. J., Crown, S. E., and Handel, T. M. (2007) Chemokine. Receptor structure, interactions, and antagonism. *Annu. Rev. Immunol.* **25,** 787–820
43. Brogden, K. A. (2005) Antimicrobial peptides. Pore formers or metabolic inhibitors in bacteria? *Nat. Rev. Microbiol.* **3,** 238–250
44. de Leeuw, E., Burks, S. R., Li, X., Kao, J. P., and Lu, W. (2007) Structure-dependent functional properties of human defensin 5. *FEBS Lett.* **581,** 515–520
45. de Leeuw, E., Li, C., Zeng, P., Li, C., Diepeveen-de Buin, M., Lu, W. Y., Breukink, E., and Lu, W. (2010) Functional interaction of human neutrophil peptide-1 with the cell wall precursor lipid II. *FEBS Lett.* **584,** 1543–1548
46. Breukink, E., Wiedemann, I., van Kraaij, C., Kuipers, O. P., Sahl, H., and de Kruijff, B. (1999) Use of the cell wall precursor lipid II by a pore-forming peptide antibiotic. *Science* **286,** 2361–2364
47. Hasper, H. E., Kramer, N. E., Smith, J. L., Hillman, J. D., Zachariah, C., Kuipers, O. P., de Kruijff, B., and Breukink, E. (2006) An alternative bactericidal mechanism of action for lantibiotic peptides that target lipid II. *Science* **313,** 1636–1637
48. Schneider, T., Kruse, T., Wimmer, R., Wiedemann, I., Sass, V., Pag, U., Jansen, A., Nielsen, A. K., Mygind, P. H., Raventós, D. S., Neve, S., Ravn, B., Bonvin, A. M., De Maria, L., Andersen, A. S., Gammelgaard, L. K., Sahl, H. G., and Kristensen, H. H. (2010) Plectasin, a fungal defensin, targets the bacterial cell wall precursor Lipid II. *Science* **328,** 1168–1172
49. Schmitt, P., Wilmes, M., Pugnière, M., Aumelas, A., Bachère, E., Sahl, H. G., Schneider, T., and Destoumieux-Garzón, D. (2010) Insight into invertebrate defensin mechanism of action. Oyster defensins inhibit peptidoglycan biosynthesis by binding to lipid II. *J. Biol. Chem.* **285,** 29208–29216
50. Sass, V., Schneider, T., Wilmes, M., Körner, C., Tossi, A., Novikova, N., Shamova, O., and Sahl, H. G. (2010) Human β-defensin 3 inhibits cell wall biosynthesis in Staphylococci. *Infect. Immun.* **78,** 2793–2800
51. Deleted in proof
52. Hornef, M. W., Pütsep, K., Karlsson, J., Refai, E., and Andersson, M. (2004) Increased diversity of intestinal antimicrobial peptides by covalent dimer formation. *Nat. Immunol.* **5,** 836–843
53. Taylor, K., McCullough, B., Clarke, D. J., Langley, R. J., Pechenick, T., Hill, A., Campopiano, D. J., Barran, P. E., Dorin, J. R., and Govan, J. R. (2007) Covalent dimer species of beta-defensin Defr1 display potent antimicrobial activity against multidrug-resistant bacterial pathogens. *Antimicrob. Agents Chemother.* **51,** 1719–1724